ELSEVIER

Cold Regions Science and Technology 26 (1997) 137–152

cold regions science and technology

Statistical effects on the evolution of compliance and compressive fracture stress of ice

Jinkoo Kim [a,*], S. Shyam Sunder [b]

[a] *Institute of Technology, Samsung Engineering and Construction, San 25, Gongseri, Yongin, Gyung-Gi Do, South Korea*
[b] *National Institute of Standard and Technology, Building and Fire Research Laboratory, Building 226, Room B354, Gaithersburg, MD 20899-0001, USA*

Received 24 October 1995; accepted 25 April 1997

Abstract

The large scatter in the experimental data of ice is partly due to the difference in the microstructure. The micromechanical damage model of Wu and Shyam Sunder [Wu, M.S., Shyam Sunder, S., 1992. Elastic anisotropy and micro-damage processes in polycrystalline ice, Part I. Theoretical formulation. Int. J. Fracture 55, 223–243.] is used to investigate the statistical effects caused by the randomness in the microstructural properties such as: microcrack length, grain size and crystallographic orientation. Probability density functions are constructed from experimental data to represent the distribution of parameters, and are used to predict the evolution of the compliance. A probability theory is used to formulate the probabilistic distribution of the failure stress and the compliance caused by the distribution of the underlying microstructural parameters. The 10 to 90th percentiles of the failure stress obtained from the model analysis reasonably match with the scatter in the given experimental data. © 1997 Elsevier Science B.V.

Keywords: microcrack; fracture stress; evolution of compliance; statistical distribution

1. Introduction

As the peak pressure of ice occurs at the ductile to brittle transition regime of loading, to investigate the deformation behavior in this region is very important for the engineering application. According to the experiments on ice the deformation behavior of ice in the ductile–brittle transition and brittle region is dominated by the nucleation and propagation of microcracks.

Experimental studies of cracking in ice have been undertaken by Gold (1972) for columnar-grained S2 ice, and by Cole (1986, 1989) for polycrystalline ice. Cole (1989) identified four distinctive stages in the compressive failure process in the brittle regime: (1) elastic stage, (2) onset of crack nucleation and the increase of crack population, (3) end of nucleation and maintenance of stability, and (4) sudden and complete failure of the specimen. From these observation, it can be concluded that there is a distinct beginning and an end to the crack nucleation process prior to brittle compressive failure.

* Corresponding author. Tel.: +82 (331) 289-6782; Fax: +82 (331) 289-6767; e-mail: jinkoo@cicgw.sce.samsung.co.kr

0165-232X/97/$17.00 © 1997 Elsevier Science B.V. All rights reserved.
PII S0165-232X(97)00013-X

In a uniaxial tension test, the first crack to nucleate from the most favorably oriented precursor generally leads to sudden failure in the ductile to brittle transition and brittle regimes. In compression, sequential crack nucleation leads to a distribution of microcracks and progressive material damage. In general there are two types of failure modes for ice under compressive loading: shear faulting and axial splitting. Shear faulting occurs when the nucleated cracks link together to form a localized shear band. Axial splitting occurs when appropriately located cracks propagate rapidly through the specimen. The failure modes are known to be independent of the temperature and the grain size, but dependent on the end conditions and lateral confinement. Schulson (1990) noted that shear faults occur when the specimens are compressed between bonded end caps, whereas splitting occurs when the specimens are compressed between brushes. In biaxial compression tests of columnar S2 ice, the direction of the ice columns and the magnitude of the confinement are important in determining the failure mode. Smith and Schulson (1993) find that under zero across-column confinement and complete along-column confinement, failure occurs by splitting. Under a low degree of across-column confinement, failure occurs by shear faulting in the loading plane. At higher levels of across-column confinement, the specimen fails by out of surface fracture. Generally the failure strength corresponding to splitting is lower than the strength for a faulting type failure as might be expected. This is consistent with the observation that ice which fails by splitting has lower crack density, i.e. less energy from external loading is consumed by the crack nucleation process prior to final fracture. The same observation can be made in the higher strain rate tests which also show lower fracture stress.

Based on physical processes of ice, Wu and Shyam Sunder (1992) proposed a microstructural model of damage evolution based on the elastic anisotropy mechanism in ice. They stipulated the existence of a starter crack or a precursor in grain boundary triple junctions and included the influence of the microstructural stress which helps the precursor propagate into a microcrack when a fracture criterion is satisfied. The microstructural model is combined with macroscopic constitutive law by Horii and Nemat-Nasser (1983) to make the evolution equation of compliance due to growing number of microcracks. In their computation, the grain size and the microcrack length are held fixed, and the basal plane and the precursor orientation are assumed to be uniformly distributed.

In reality, however, there are many sources of statistical variation in the microstructure of ice. From experiments on compressive fracture of ice, Schulson (1990) suggested that the large scatter in the brittle compressive fracture stress, compared with the smaller degree of scatter in the ductile peak compressive strength, is more a characteristic of brittle behavior of ice than a manifestation of experimental error. The large distribution in micromechanical parameters makes it necessary to use the statistical expression in the quantitative representation of the numerical results.

Considering the fact that the grain size is not constant even in the ice made under laboratory-controlled condition, Wu and Shyam Sunder (1992) included the probability density function (PDF) of crack length and grain size in their damage model to show the effect of variation of the parameters on the evolution of compliance. They used two parameter gamma distribution to model the distribution of grain size. The distribution of crack length is determined from the linear relation between grain size and crack length proposed by Cole (1986). The probability density functions of the grain size satisfy the mathematical requirements they need, but they are not based on experimental data. Furthermore, as the change in compliance is shown after the averaging process, the amount of scatter of the resultant compliance caused by the variation of the input parameters is still unknown.

In this study, the PDF of the grain size variation is obtained based on the histogram constructed from an ice thin section photograph. The PDF of crack length is obtained from the histogram of the crack length normalized by the mean grain size constructed by Cole (1986) from experiments of about 40 ice specimens. These density functions are used in the formulation for the evolution and variation of the compliance. Also the effect of the non-uniform distribution of the basal plane orientation on the evolution of compliance is investigated. It is interesting to note that the formulation of the evolution equation considering non-uniform distribution of the basal plane leads to the damage modeling of the S3 ice which is a special type of columnar grained ice.

2. Description of the micromechanical model

The proposed model incorporates the microstructural stress caused by the elastic anisotropy as well as the Coulombic friction between crack faces in the analysis. A microcrack is assumed to nucleate from a precursor which forms at the triple junction of grain boundaries due to the elastic property mismatch between the grains. As the loading increases more and more precursors nucleate into microcracks, resulting in accumulation of damage. The macroscopic damage evolution is computed by the method of Horii and Nemat-Nasser (1983) which analyzes the contribution of individual cracks in an effective medium. The final failure is defined when one of the most favorably oriented microcracks propagates unstably. The maximum principal tensile stress criterion of Erdogan and Sih (1963) is used for both nucleation and propagation of the microcracks.

2.1. Microstructural stresses and the precursor formation

The microstructural stresses are made up of a uniform component and a non-uniform component with singularity (Evans, 1978). The uniform component σ_0 results from the mismatch in property between the two adjacent grains adjoining the grain boundary, and is the first order approximation of the total stress computed by the procedure developed by Eshelby (1957), which is:

$$\sigma_0 = \tfrac{1}{2}\{[\mathbf{C}_g(\zeta_1) + \mathbf{C}_g(\zeta_2)\mathbf{S} - 2\mathbf{I}]\}\sigma_a \tag{1}$$

where $\mathbf{C}_g$ is the stiffness matrix of single ice crystals in the global reference frame. ζ_1 and ζ_2 denote the basal plane orientations of the adjoining grains shown in Fig. 1. The matrix $\mathbf{S}$ represents the compliance matrix of the polycrystal, and σ_a is the applied remote stress field. The total stress is the summation of the remote stress and the microstructural stress. The compliance matrix of a single ice crystal determined by Gammon et al. (1983) at temperature $T = -16°C$ are given as follows:

$$[S_g] = \begin{bmatrix} 1.0318 & -0.2316 & -0.4287 & & & \\ & 0.8441 & -0.2316 & & 0 & \\ & & 1.0318 & & & \\ & & & 3.3719 & & \\ & \text{sym} & & & 2.9210 & \\ & & & & & 3.3179 \end{bmatrix} 10^{-1}\ \text{GPa}^{-1} \tag{2}$$

where the plane of the transverse isotropy is contained in the X_1–X_3 plane, and the c-axis is in the X_2 direction. The stiffness matrix of a single ice crystal can be obtained by inverting the compliance matrix. The elastic

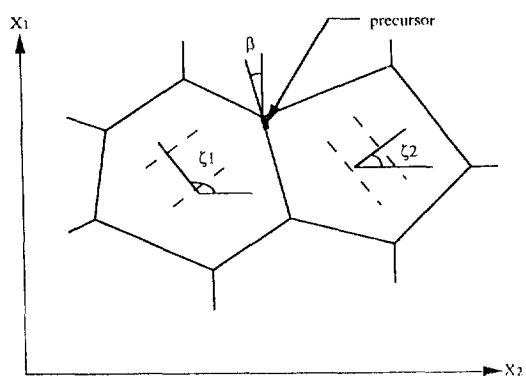

Fig. 1. Orientation of basal plane and precursor crack in an ice polycrystal.

constants of polycrystalline ice are determined by the distribution of the crystallographic orientation of each grain. The undamaged compliance matrix of isotropic granular ice at $-16°C$ are (Gammon et al., 1983)

$$[S] = \begin{bmatrix} 1.0716 & -0.3486 & -0.3486 & & & \\ & 1.0716 & -0.3486 & & 0 & \\ & & 1.0716 & & & \\ & & & 2.8401 & & \\ & \text{sym} & & & 2.8401 & \\ & & & & & 2.8401 \end{bmatrix} 10^{-1}\ \text{GPa}^{-1} \tag{3}$$

2.2. Nucleation of microcracks

The formulation of a microcracking procedure takes into account the combined stress field generated by both the applied and the microstructural stress. Consider the precursor which is oriented at an angle β with the X_1 axis and is subjected to the total remote normal stress σ'_{11} and shear stress σ'_{11} defined in a local coordinate X'_1–X'_2:

$$\sigma'_{11} = (\sigma_{22} + \sigma_{11})/2 + [(\sigma_{22} - \sigma_{11})/2]\cos 2\beta - \sigma_{12}\sin 2\beta\ \sigma'_{12} = -[(\sigma_{22} - \sigma_{11})/2]\sin 2\beta - \sigma_{12}\cos 2\beta \pm \mu\sigma'_{11} \tag{4}$$

where μ is the coefficient of friction and $\mu\sigma'_{12}$ is the Coulombic frictional stress which oppose sliding when the normal stress is compressive. The effective shear stress σ'_{12} is set to zero when the applied stress is smaller than or equal to the frictional stress. The mode I and II stress intensity factors become

$$K_{\mathrm{I}} = \sigma'_{11}\sqrt{\pi a}\ \ K_{\mathrm{II}} = \sigma'_{12}\sqrt{\pi a} \tag{5}$$

where a is the half precursor length. If the normal stress is compressive, it is assumed that the crack is closed and consequently $K_{\mathrm{I}} = 0$. The asymptotic distribution of the tangential and shear stresses can be expressed as follows:

$$\sigma_{\theta\theta} = \frac{1}{\sqrt{2\pi r}}\cos\frac{\theta}{2}\left[K_{\mathrm{I}}\cos^2\frac{\theta}{2} - \frac{3}{2}K_{\mathrm{II}}\sin\theta\right]\ \ \sigma_{r\theta} = \frac{1}{2\sqrt{2\pi r}}\cos\frac{\theta}{2}\left[K_{\mathrm{I}}\sin\theta + K_{\mathrm{II}}(\cos\theta - 1)\right] \tag{6}$$

where r is the radial distance from the tip of the precursor and θ is the angle measured anti-clockwise from a line extending along the precursor in the solid.

The maximum principal tensile stress criterion is used as a crack nucleation criterion, which stipulates that a precursor extends into a microcrack when the following expression reaches the microscopic fracture fracture toughness k_{IC}:

$$K_{\mathrm{I}}\cos^3\frac{\theta_{\mathrm{m}}}{2} - 3K_{\mathrm{II}}\cos^2\frac{\theta_{\mathrm{m}}}{2}\sin\frac{\theta_{\mathrm{m}}}{2} = k_{\mathrm{IC}} \tag{7}$$

where θ_{m} is obtained by setting the $\sigma_{r\theta}$ in Eq. (6) equal to zero, which is given by

$$\tan\frac{\theta_{\mathrm{m}}}{2} = \tfrac{1}{4}\left[\frac{K_{\mathrm{I}}}{K_{\mathrm{II}}} \pm \sqrt{\left(\frac{K_{\mathrm{I}}}{K_{\mathrm{II}}}\right)^2 + 8}\right] \tag{8}$$

The microstructural fracture toughness k_{IC} is determined from the effective surface energy γ, the Young modulus E, and the Poisson ratio v:

$$k_{\mathrm{IC}} = \sqrt{2E\gamma}\ \text{plane stress}\ \ k_{\mathrm{IC}} = \sqrt{\frac{2E\gamma}{(1 - v^2)}}\ \text{plane stress} \tag{9}$$

The value of γ depends on whether the precursor extends along the grain boundary or into the crystal. In this study the extension into the crystals is assumed and the solid vapor surface energy determined to be 0.109 J m^{-2} by Ketcham and Hobbs (1969) is used.

Eq. (8) yields two critical initial angles and the angle that yields the most positive value in Eq. (7) is chosen and compared with k_{IC}. Eq. (7) represents the kinetic law of microcracking evolution, and as the applied stress is increased nucleation maps can be plotted in the β–ζ space. The precursor extends in a direction perpendicular to the maximum tangential stress and the crack path analysis requires an evaluation of the stress field around a precursor at each nucleation site (β, ζ, d) where the microcracking criterion is satisfied.

The resulting crack profiles are generally curved and approximated by straight lines of orientation χ (see Wu and Shyam Sunder (1992)).

2.3. Elastic compliance of a damaged solid

The damaged compliance **S** can be computed using the theory developed by Horii and Nemat-Nasser (1983). It can be divided into the original compliance $\mathbf{S}_0$ and the additional compliance **H** generated from the nucleation of the microcracks:

$$\mathbf{S} = \mathbf{S}_0 + \mathbf{H} \tag{10}$$

The plane stress representation of the undamaged compliance is given by the following matrix:

$$[S] = -\frac{1}{E}\begin{bmatrix} 1 & -\upsilon & 0 \\ -\upsilon & 1 & 0 \\ 0 & 0 & 2(1+\upsilon) \end{bmatrix} \tag{11}$$

where E and υ denote the Young modulus and the Poisson ratio, respectively. The additional compliance **H** can be expressed as following when the crack length and the grain size are constant, and the orientations of the precursor and the basal plane are uniformly distributed from 0 to π:

$$H_{ij} = \frac{M}{\pi^2}\int\int K'_{kl} T_{ki} T_{lj} \mathrm{d}\zeta \mathrm{d}\beta \tag{12}$$

where $M = 12/\pi d^2$ represents the maximum number of precursors per unit area in the given stress assuming that there are maximum number of 2 precursors per grain and the number of microcracks per grain is $6/\pi d^2$ (Cole, 1986), and K' is the single crack contribution to the additional compliance given in Horii and Nemat-Nasser (1983).

2.4. Fracture stress

Under the strain rates greater than the ductile to brittle transition, the strength of ice depends on the nucleation and/or propagation of the microcracks. In tension the first crack nucleation from a favorably oriented precursor generally leads to a sudden failure. But in compression the sequential nucleation leads to distributed cracking and progressive material damage. When ice is loaded with uniaxial compression it fails by an axial splitting, whereas under biaxial compression the nucleated cracks link together to form a localized shear band. In this study the maximum principal tensile stress criterion is used to predict the brittle failure of ice.

Once a microcrack nucleates from a precursor, it remains stable until a further loading causes the microcrack to propagate. To obtain the fracture stress the crack length c and the orientation χ are used in Eqs. (4) and (5) instead of the precursor length a and orientation β. The microscopic fracture toughness is replaced by the macroscopic fracture toughness measured by Nixon and Schulson (1987) in Eq. (7). It ranges from 0.08 to 0.13 MPa $m^{0.5}$ as the temperature changes from $-2°$ to $-50°$C. The macroscopic fracture toughness is independent

of the strain rate, and is 2–3 times higher than the microscopic toughness measure. When Eq. (7) is satisfied after the above adjustments, the total stress at failure σ_f becomes

$$\sigma_{f(11)} = \frac{K_{IC}}{\sqrt{\pi c}} \frac{1}{\left[\frac{1+\lambda}{2} - \frac{1-\lambda}{2}\cos 2\chi\right]\cos^3\frac{\theta_m}{2} - 3\left[\frac{1-\lambda}{2}\sin 2\chi \pm \mu\right]\cos^2\frac{\theta_m}{2}\sin\frac{\theta_m}{2}} \tag{13}$$

where K_{IC} is the macroscopic fracture toughness and λ is the confinement ratio.

It should be acknowledged that the failure process of ice is so complicated that it is difficult to consider all the mechanisms involved in the simple model. The process is highly influenced by various factors such as confining pressures, strain rates and microstructure of ice, etc. In many cases the failure is caused by the connection of more than one crack, not by the unstable propagation of a single crack as prescribed in this study. The failure model presented in this study is based on the theory of linear elastic fracture mechanics and may be more precisely applied to brittle materials such as glass, ceramic, etc. However, as suggested by Schulson (1990), it is reasonable to predict the failure stress of ice with such an approach when the strain rate is fast enough and the ice shows pseudo-brittle behavior.

3. Effect of the statistical distribution of microstructures

3.1. Variation of microcrack length

In this section, the scatter of the failure stress and the compliance is predicted based on the scatter of the microstructural parameters. For that purpose, the PDF of the crack length and the grain size are obtained from experimental data, and they are used to get the probability density function of the failure stress and the additional compliance through a simple probability theory.

The size of a crack at a given temperature depends on the applied stress and the microstructural characteristics of the polycrystalline aggregate, such as the orientation, shape and size of the grains. Under certain conditions, these cracks propagate only a short distance before coming to rest within the material. Given sufficiently high stress levels, the cracks can propagate through the material to cause brittle fracture. In compression, when cracks do not propagate, they are responsible for the gradual weakening of the structure as straining proceeds.

A significant relationship between the grain size and the internal cracking of polycrystalline ice has been reported (Cole, 1986). Cole showed the average crack length plotted against the average grain diameter, along with the least-squares best fit curve for all data points. He also showed a histogram of all the crack length data normalized by the mean grain size, which is reproduced in Fig. 2. The distribution of the merged normalized data retains essentially the same shape as the raw crack length data of the individual specimens. Given the observation, it appears likely that a generalized distribution in terms of normalized crack length may be used to estimate the actual crack length distribution for any given mean grain size without any computational effort.

The PDF of the normalized crack length can be obtained by fitting the given histogram to one of the existing density functions. Two parameter Weibull distribution is applied first for that purpose because it has advantage in fitting the numerical data. If α and β are taken as its parameters, its functional form is given by

$$f_X(x) = \alpha\beta^{-\alpha}x^{\alpha-1}\exp(-\beta^{-\alpha}x^{\alpha}) \quad x>0, \alpha>0, \beta>0 \tag{14}$$

where $x = 2c/d$ in this case. Weibull distribution has an explicit expression for the cumulative distribution function (CDF), which is

$$F_X(x) = 1 - \exp(-\beta^{-\alpha}x^{\alpha}) \tag{15}$$

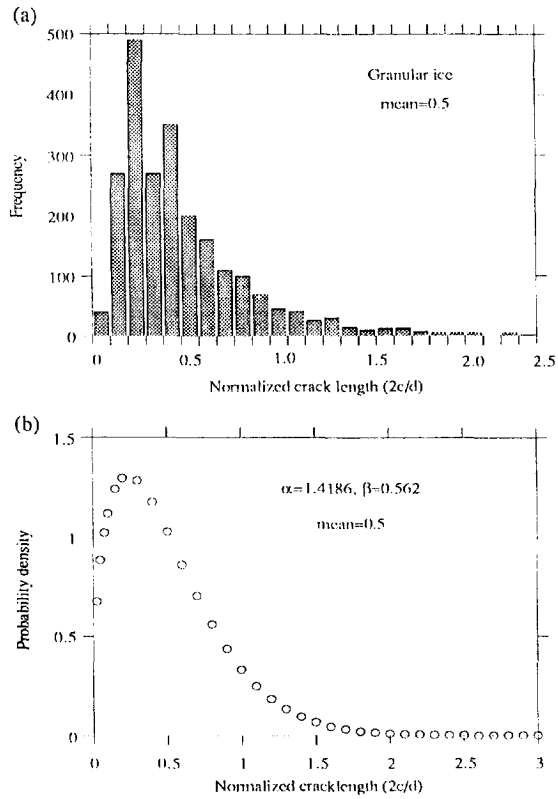

Fig. 2. (a) Histogram of normalized crack length from Cole (1986). (b). Weibull distribution fit of the normalized crack length with the parameters $\alpha = 1.4186$, $\beta = 0.562$.

Estimation of the parameters α and β of the Weibull distribution is somewhat difficult to do. There exist analytical methods for estimating parameters, but a more rapid and commonly used method, based on a graphical technique, is used here. This method is based on the fact that the CDF of the Weibull distribution can be transformed into a linear function of log x by means of a double-logarithmic transformation:

$$\log\left[\ln\frac{1}{1-F_X(x)}\right] = \alpha \log x - \alpha \log \beta \tag{16}$$

and it can be seen that the right-hand side is linear in log x. If the given data points fall reasonably close to a straight line after this transformation, it can be assumed that the underlying distribution follows the Weibull type distribution. The parameters of this distribution can be estimated by applying the linear regression method to fit a straight line to the transformed data. Fig. 2b shows the probability density function of the normalized crack length x obtained by the above procedure. Once the PDF of the normalized crack length is found, the PDF of the crack length with constant grain size can be obtained through the following relation:

$$f_C(c) = \frac{dx}{dc} f_X = \alpha\left(\frac{\beta d}{2}\right)^{-\alpha} c^{\alpha-1}\exp\left[-\left(\frac{\beta d}{2}\right)^{-\alpha} c^{\alpha}\right] \tag{17}$$

which is also a Weibull distribution with parameter α and $\beta d/2$.

The Weibull distribution was quite useful in most cases. But for the distribution of the failure strength due to the grain size distribution the log-normal distribution turned out to provide a better fit for the numerical results. The functional form of the log-normal distribution is

$$f_X(x) = \frac{1}{\sqrt{2\pi\beta}} x^{-1} \exp\left[-\frac{(\ln x - \alpha)^2}{2\beta^2} \right] \tag{18}$$

where α and β are the parameters of the function. The probability that a random variable having the log-normal distribution will take on a value between a and b $(0 < a < b)$ can be obtained by

$$\int_a^b \frac{1}{2\pi\beta} x^{-1} \exp\left[-\frac{(\ln x - \alpha)^2}{2\beta^2} \right] \mathrm{d}x = F\left(\frac{\ln b - \alpha}{\beta} \right) - F\left(\frac{\ln a - \alpha}{\beta} \right) \tag{19}$$

where F is the cumulative distribution function (CDF) of the standard normal distribution.

The PDF of the additional compliance **H** considering the distribution of the crack length is obtained using the fact that **H** is the monotonically increasing function of the crack length:

$$f_H(H_{ij}) = \frac{1}{\dfrac{\mathrm{d}H_{ij}}{\mathrm{d}c}} f_C(c) \tag{20}$$

where discrete values of $\mathrm{d}H_{ij}/\mathrm{d}c$ are obtained from the model analysis with various microcrack lengths, and the data are fit to a functional form to obtain a probability density function of additional compliance.

When the crack length has a certain distribution $f_C(c)$, the evolution equation for the additional compliance (Eq. (12)) becomes

$$H_{ij} = \frac{M}{\pi^2} \int\int\int K'_{kl} T_{ki} T_{lj} f_C(c) \mathrm{d}\zeta \mathrm{d}\beta \mathrm{d}c \tag{21}$$

where the effect of the crack length variation is considered by spatial average process.

Similarly, the scatter in the experimental data of the fracture stress may be predicted through the PDF of the failure stress. When the PDF of the microcrack length is known and the grain size is assumed to be constant, the PDF of the failure stress is obtained by

$$f_\Sigma(\sigma_f) = \frac{1}{\dfrac{\mathrm{d}\sigma_f}{\mathrm{d}c}} f_C(c) \tag{22}$$

where $\mathrm{d}\sigma_f/\mathrm{d}c$ is obtained from the model analysis.

3.2. Grain size variation

To know the grain size distribution in ice, the grain size histograms are constructed from thin section photographs of freshwater granular ice (Fig. 3) and columnar S2 ice (Fig. 4). Averaged grain sizes of 4.5 and 4.8 mm are obtained from the histograms although they are reduced to 4.2 and 4.6, respectively, when the histograms are fit into the Weibull distribution functions.

The CDF of the additional compliance which is now a function of the microcrack length and the grain size can be obtained by integrating the joint probability density function:

$$F_H(\overline{H}_{ij}) = \int\int f_{C,D}(c,d) \mathrm{d}c \mathrm{d}d \tag{23}$$

where the integration is performed in the domain of the crack length and the grain size that satisfy

$H_{ij}(c,d) \leq \overline{H}_{ij}$. The joint probability density function $f_{C,D}(c,d)$ is obtained from the following relation:

$$f_{C,D}(c,d) = f_{C|D}(c|d) f_D(d) = f_{\underline{C}}\left(\frac{c}{d}\right)\frac{f_D(d)}{d} \tag{24}$$

The numerical evaluation of the cumulative density function, Eq. (23), is not easy to carry out, thus in this study the PDF of the additional compliance is obtained from an approximate formulation. In a two-dimensional case, the crack length term can be separated from the expression of the additional compliance:

$$H_{ij} = \kappa_{ij} c^2 \tag{25}$$

where κ_{ij} is the additional compliance divided by the square of the crack length. In the self-consistent model of Wu and Shyam Sunder (1992) the damaged compliance is used in the calculation of the additional compliance H_{ij}, so the crack length term appears in both sides of Eq. (14) and κ_{ij} is the implicit function of the crack length. Because of this reason, the non-interactive model is used in this analysis, in which the additional compliance due to a crack nucleation is analyzed in a medium with the original compliance. The use of non-interactive model results in a little stiffer response of the material compared with the use of the self-consistent method.

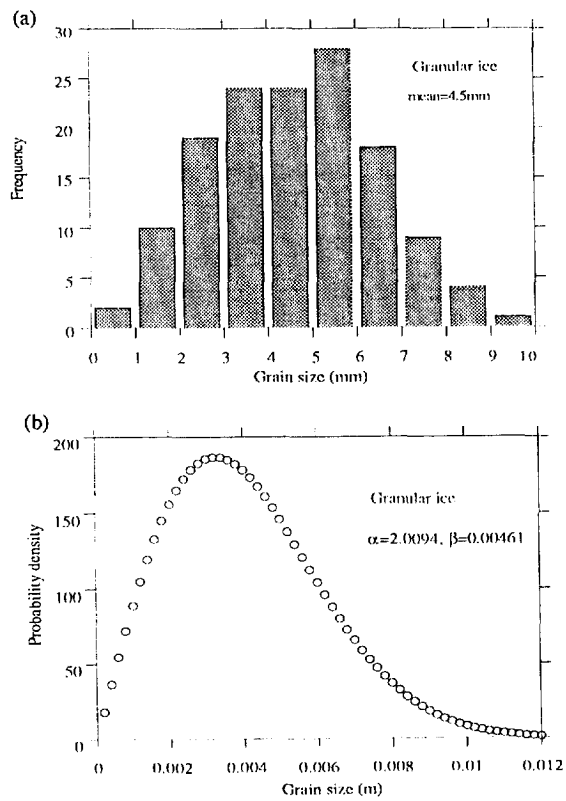

Fig. 3. (a) Grain size histogram constructed from a thin section photograph of granular ice. (b). Weibull distribution fit of the grain size histogram.

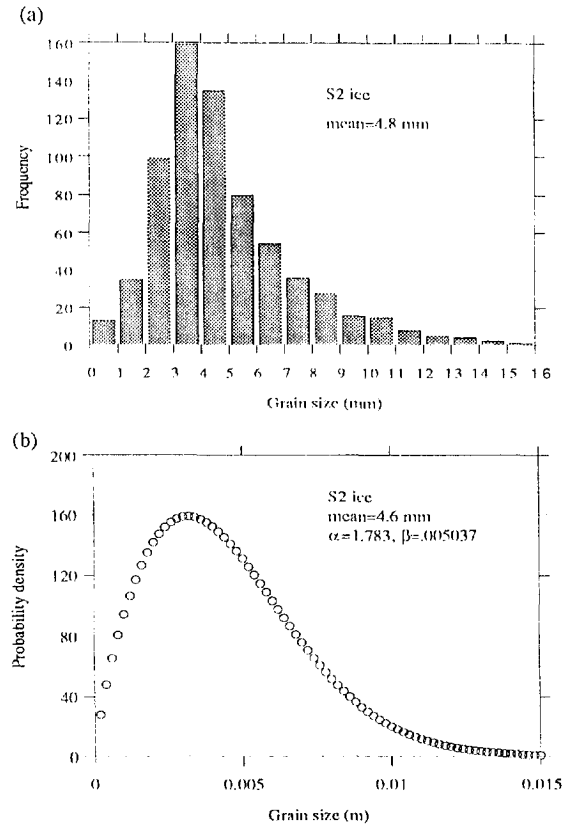

Fig. 4. (a) Grain size histogram of a S2 ice. (b) Weibull distribution fit of the histogram.

With the CDF of the crack length distribution obtained from Eqs. (15) and (17), the PDF of the additional compliance is calculated from the probability theory as following:

$$F_H(H_{ij}) = \int f_D(d) F_C(c)\mathrm{d}d = \int f_D(d) F_C\left(\sqrt{\frac{H_{ij}}{\kappa_{ij}}}\right)\mathrm{d}d \tag{26}$$

$$f_H(H_{ij}) = \frac{\mathrm{d}}{\mathrm{d}H_{ij}} F_H(H_{ij}) \tag{27}$$

where κ_{ij} is assumed to be the function of only the grain size d and should be calculated from the model analysis.

With the variation of the grain size and the crack length, the equation for the additional compliance is now modified to

$$H_{ij} = \frac{1}{\pi^2}\int\int\int\int MK'_{kl}T_{ki}T_{lj}f_C(c)f_D(d)\mathrm{d}\zeta\,\mathrm{d}\beta\,\mathrm{d}c\,\mathrm{d}d \tag{28}$$

In the above expression, the additional compliance is averaged over the possible range of the crack length and the grain size variation.

To obtain the PDF of failure stress considering the simultaneous distributions of crack length and the grain size is very difficult, so in this study the crack length is assumed to be proportional to the grain size. With such

an assumption, the probability density function of the failure strength is obtained from the PDF of the grain size with the crack length proportional to the grain size:

$$f_\Sigma(\sigma_f) = \frac{1}{\frac{d\sigma_f}{dd}} f_D(d) \tag{29}$$

3.3. Non-uniform distribution of basal plane and precursor orientation

It is widely acknowledged that the fabric orientation strongly influences the elastic moduli of ice. In granular ice, the basal plane orientations tend to be randomly distributed in all directions, especially before the ice undergoes any loading. Thus it is assumed in the calculation of the compliance that the basal plane and the precursor orientations are uniformly distributed on the two-dimensional plane. In columnar grained ice, three types of ice, S1, S2 and S3 ice, can be distinguished according to the basal plane orientation. In S1 ice, the preferred crystallographic orientation of the c-axis is vertical, i.e. perpendicular to the ice cover. In S2 ice, the c-axis orientation is horizontal and randomly distributed. In the presence of strong currents, while the c-axis

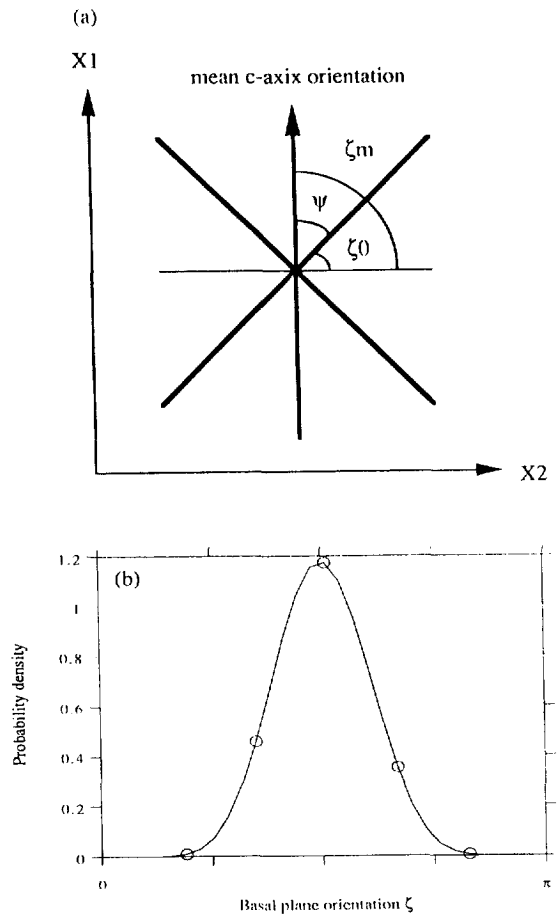

Fig. 5. (a) Distribution of the c-axis (basal plane) orientation around the mean value (ζ_m is the orientation of the mean c-axis and ψ is the scatter angle). (b) Beta distribution of the c-axis distribution from 0 to τ with the distribution parameter $n = 10$.

may still be located in the horizontal plane, a preferred orientation may develop. This type of ice is classified as S3 ice.

In general, the distribution of c-axis orientation is confined to a range of angles $|\zeta_m - \psi \le \zeta \le |\zeta_m + \psi|$ as shown in Fig. 5, where ζ_m is the orientation of the mean c-axis and ψ is the scatter angle. An appropriate PDF for idealization of the c-axis distribution is the symmetric beta distribution, and the probability density function has the form:

$$f_Z(\zeta) = \frac{1}{B_n \pi^{2n+1}} [\zeta - (\zeta_m - \psi)]^n [\zeta_m + \psi - \zeta]^n \text{ for } \zeta_m - \psi \le \zeta \le \zeta_m + \psi = 0 \text{ elsewhere} \quad (30)$$

where $B_n = n!n!/2n + 1!$

Fig. 6 shows an example of the beta distribution with $n = 10$, the mean c-axis orientation $\zeta_m = \pi/2$ and the scatter angle $\psi = \pi/2$.

The original compliance of S3 ice can be computed after spatially averaging the value at each crystal orientation by multiplying the relative frequency of that orientation:

$$S_{ij} = \int S_{gij}(\zeta) f_Z(\zeta) d\zeta \quad (31)$$

where S_{gij} is the compliance matrix of a single crystal with c-axis oriented at ζ in the local coordinate system,

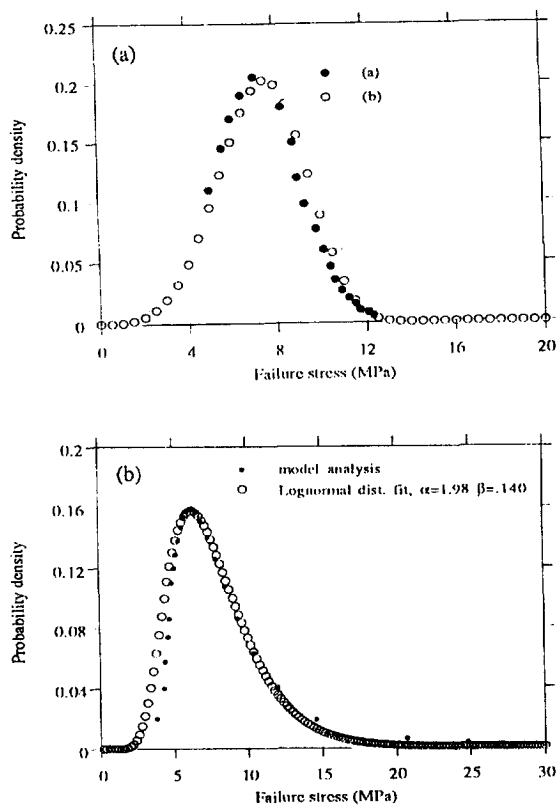

Fig. 6. Weibull distribution fit of the PDF of failure stress of granular ice considering crack length distribution at $d = 4$ mm ($\alpha = 4.33$ $\beta = 8.088$). (6) Log-normal distribution fit considering grain size distribution with crack length proportional to the grain size ($\alpha = 1.98$, $\beta = 0.14$).

and $f_Z(\zeta)$ is the PDF of the c-axis orientation. The crystal elastic compliance at a given orientation can be determined by the following coordinate transformation of the matrix in the principal directions of the crystal:

$$\mathbf{S}_g = \mathbf{R}^T \mathbf{S}_g \mathbf{R} \tag{32}$$

where $\mathbf{R}$ is the rotation matrix based on the direction cosines of the c-axis, $\mathbf{R}^T$ is the transpose of the rotation matrix and $\mathbf{S}_g$ is the compliance matrix of a single crystal in the principal coordinate system (see Wu and Shyam Sunder, 1991).

An example of the plane stress compliance matrix of S3 ice is computed by the above method using $n = 10$ at $T = -16°C$ which is:

$$S_{ij} = \begin{bmatrix} 1.0773 & -0.2859 & 0 \\ -0.2859 & 0.9193 & 0 \\ 0 & 0 & 2.9787 \end{bmatrix} \times 10^{-1}\ \text{GPa}^{-1} \tag{33}$$

Similarly, the compliance of S2 ice can be computed using the uniform distribution of basal plane orientation ($n = 0$), which is

$$[S_{ij}] = \begin{bmatrix} 1.0603 & -0.3539 & 0 \\ -0.3539 & 1.0603 & 0 \\ 0 & 0 & 2.8286 \end{bmatrix} \times 10^{-1}\ \text{GPa}^{-1} \tag{34}$$

4. Numerical results

In this study, the statistical variation of the failure stress and the additional compliance caused by the variation of the underlying microstructural parameters are demonstrated through the 10 to 90th percentiles of the probability density functions. The distribution functions of the geometric parameters are obtained from experimental observation and are used as a weighting function in the computation of the total compliance. A simple probability theory is applied to the results from the model analysis to obtain the PDFs of the resulting failure stress and compliance.

Fig. 6 shows the numerically obtained PDF of failure stress and the appropriate fit by Weibull and the log-normal density function. The probability densities are obtained from Eqs. (22) and (29) using various values of crack length and grain size. For the crack length distribution the PDF of the crack length is obtained from Eq. (17) with the grain size $d = 4$ mm, whereas the probability density function obtained from the grain size histogram is used for the grain size distribution case. In this case the crack length is taken to be 50% of the grain size.

Fig. 7a shows the experimental data of the brittle fracture stress of freshwater granular ice from Schulson (1990) and the analytical predictions using the mean grain size. The data were obtained under uniaxial compression at the temperature of $-10°C$ and strain rates of $10^{-3}\ s^{-1}$ for grain sizes varying from approximately 1 to 10 mm. These conditions are considered in the numerical model by setting the friction coefficient $\mu = 0.5$ and the macroscopic fracture toughness $K_{IC} = 80\ \text{kPa m}^{0.5}$. The 10 to 90th percentiles of the fracture stress obtained from the probability density functions are compared with the experimental data of Schulson and Cannon (1984) and Schulson (1990) in Fig. 7b at the mean grain size of 4 mm (crack length distribution) and 4.2 mm (grain size distribution). The length of the percentiles is consistent with the scatter of the experimental data.

Fig. 8 shows the evolution of the compliance in isotropic granular ice with (i) constant crack length and grain size, (ii) crack length variation with constant grain size, and (iii) both crack length and grain size variation. In case (i) and (ii), the grain size is set to 4.2 mm which is the mean value of the probability density function of the grain size determined from the grain size histogram (Fig. 3). In case (i), the crack length is determined from the

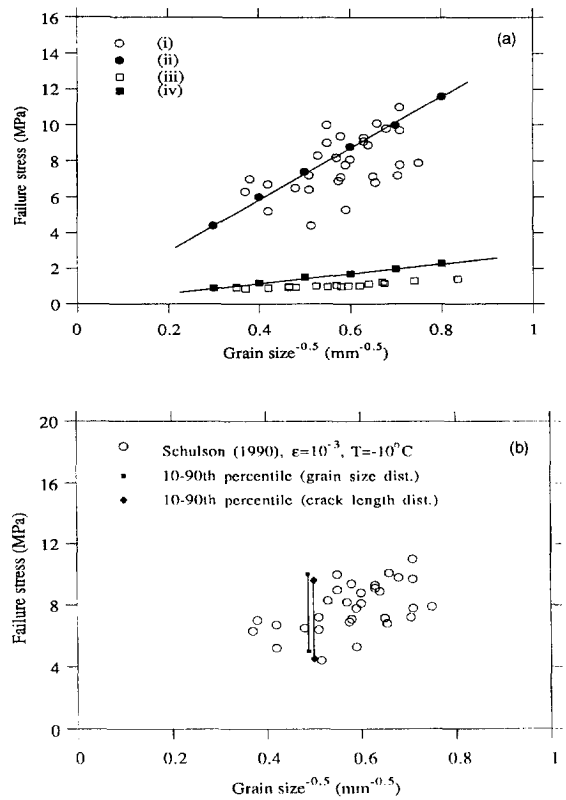

Fig. 7. (a) Comparison of model predictions for the failure stress of ice with the experimental data of Schulson (1990): (i) data from uniaxial compression tests ($T = -10°C$, $\dot{\varepsilon} = 10^{-3}$ s^{-1}); (ii) model predictions with $\mu = 0.5$, $K_{IC} = 80$ kPa m$^{0.5}$; (iii) data from uniaxial tensile tests ($T = -10°C$, $\dot{\varepsilon} = 10^{-3}$ s^{-1}); (iv) model predictions with $\mu \approx 0$, $K_{IC} = 48$ kPa m$^{0.5}$. (b) 10 to 90th percentiles of failure stress distribution considering crack length and the grain size distribution: (i) Schulson (1990); (ii) Schulson and Cannon (1984); (iii) 10–90th percentile (grain size distribution); (iv) 10–90th percentile (crack length distribution).

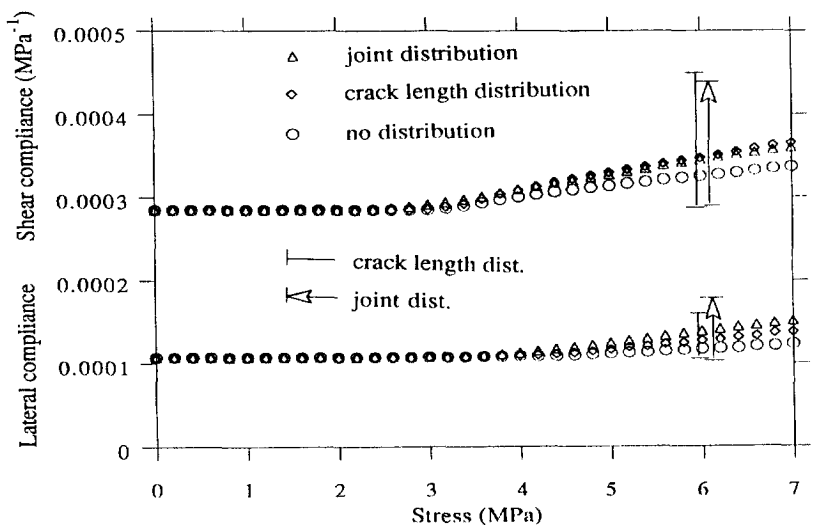

Fig. 8. Compliance evolution of granular ice with the 10 to 90th percentile of its distribution at $\sigma = 6$ MPa.

mean value of the normalized crack length histogram (Fig. 2) which is 50% of the grain size. In case (ii), the PDF of the crack length is determined from the normalized crack length histogram. For the last case, the PDF of the grain size as well as the PDF of the crack length is used in the computation of the evolution of the compliance. For each grain size the PDF of the crack length is constructed from the PDF of the normalized crack length (Eq. (17)) and is weighted by the probability of the corresponding grain size. Similar computations are conducted with the S2 ice which has the undamaged compliance of Eq. (34) (Fig. 9). The PDF of the grain size is also obtained from a thin section photograph of S2 ice. The results show that the increase of the compliance is larger in S2 ice. This may be explained by the fact that the grain size of the S2 ice is a little larger than that of the granular ice, and the PDF of S2 ice is more skewed and widely spread than that of the granular ice.

Figs. 8 and 9 also display the 10 to 90th percentiles of the compliance obtained from the corresponding CDFs of the additional compliance. The length of the percentiles represents the amount of the scatter in compliance caused by the scatter in the material parameters. At the same loading condition the length is longer in S2 ice which has a larger mean grain size and a more skewed and widely spread density function.

5. Conclusions

The following conclusions are drawn from the numerical simulation:(1) The 10 to 90th percentiles of the distribution function of the failure stress reasonably represent the scatter in experimental data obtained by Schulson (1990).(2) The scatter in the value of the parameters generally increases the rate of compliance evolution.(3) The 10th to 90th percentiles of the compliance show that the scatter in predicted failure stress increases when the parameters are more scattered and skewed.(4) The damage accumulation in the columnar S3 ice can be predicted theoretically by applying the non-uniform distribution of the c-axis orientation in the evolution equation.

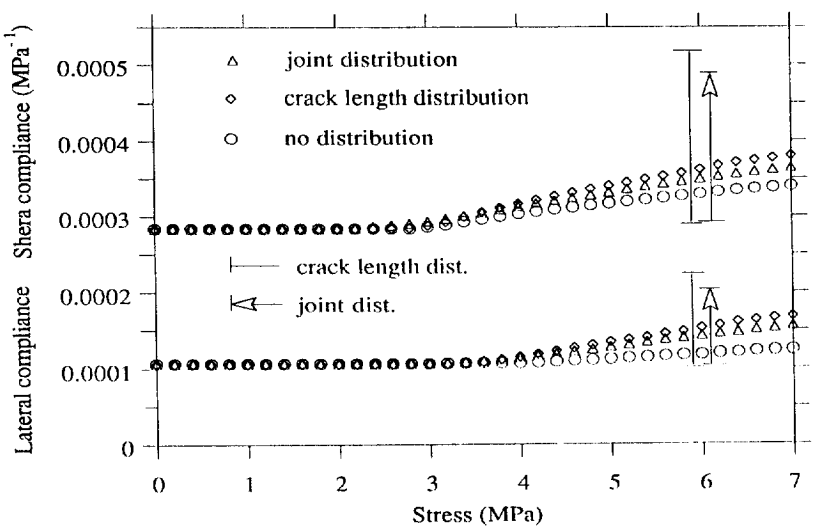

Fig. 9. Compliance evolution of S2 ice with the 10 to 90th percentile of distribution at $\sigma = 6$ MPa.

References

Cole, D.M., 1986. Effect of grain size on the internal fracturing of polycrystalline ice. CRREL REPORT 86-5, U.S. Army Cold Regions Research and Engineering Laboratory, Hanover, NH.

Cole, D.M., 1989. Microfracture and the compressive failure of polycrystalline ice. Proc. IUTAM/IAHR Symp. on Ice–Structure Interaction, p. 231.

Erdogan, F., Sih, G.C., 1963. On the crack extension in plates under plane loading and transverse shear. J. Basic Eng. 85, 519–527.

Eshelby, J.D., 1957. The determination of the elastic field of an ellipsoidal inclusion, and related problems. Proc. R. Soc. A241, 376.

Evans, A.G., 1978. Fracture in Ceramic Materials: Toughening Mechanisms, Machining Damage, Shock. Noyes Publ., Park Ridge, NJ.

Gammon, P.H., Kiefte, H., Clouter, M.J., Denner, W.W., 1983. Elastic constants of artificial and natural ice samples by Brillouin spectroscopy. J. Glaciol. 29, 433–459.

Gold, L.W., 1972. The process of failure in columnar-grained ice. Philos. Mag. 26, 311.

Horii, N., Nemat-Nasser, S., 1983. Overall moduli of solids with microcracks: load-induced anisotropy. J. Mech. Phys. Solids 31, 155–171.

Ketcham, W.M., Hobbs, P.V., 1969. An experimental determination of the surface energies of ice. Philos. Mag. A 19, 1161–1173.

Nixon, W.A., Schulson, E.M., 1987. A micromechanical view of the fracture toughness of ice. J. Phys. 48 (C1), 313–319.

Schulson, E.M., 1990. The brittle compressive fracture of ice. Acta Metall. Mater. 38 (10), 1963–1976.

Schulson, E.M., Cannon, N.P., 1984. The effect of grain size on the compressive strength of ice. Proc. IAHR Ice Symp., Hamburg, 1, pp. 29–38.

Smith, T.R., Schulson, E.M., 1993. The brittle compressive failure of fresh-water columnar ice under biaxial loading. Acta Metall. Mater. 41, 153.

Wu, M.S., Shyam Sunder, S., 1991. Effect of grain size variations on damage in polycrystalline ice. ASCE Proc. 6th Int. Cold Region Eng. Conf., Hanover, NH, pp. 542–553.

Wu, M.S., Shyam Sunder, S., 1992. Elastic anisotropy and micro-damage processes in polycrystalline ice, Part I. Theoretical formulation. Int. J. Fract. 55, 223–243.